Experimental and Theoretical Study of the Use of Multifunctional Initiators in the High Impact Polystyrene Bulk Process

E. Berkenwald,[1] M. L. Laganá,[1] J.M. Maffi,[1] P. Acuña,[2] G. Morales,[2] D. Estenoz[1,3]

[1] *Department of Chemical Engineering, Instituto Tecnológico de Buenos Aires (ITBA), Av. Madero 399, C.P.1106, Buenos Aires, Argentina*

[2] *Centro de Investigación en Química Aplicada (CIQA), Bv. E. Reyna Hermosillo 140, C.P. 25294, Saltillo, Coahuila, México*

[3] *Instituto de Desarrollo Tecnológico para la Industria Química, INTEC (Universidad Nacional del Litoral, CONICET), Güemes 3450, C.P. 3000, Santa Fe, Argentina*

The performance of three multifunctional peroxide initiators in a bulk high impact polystyrene (HIPS) process was experimentally and theoretically investigated. For the experimental work, a series of batch reactions was carried out, comprising the main stages of an industrial HIPS bulk process using multifunctional initiators with varying functionality and structure: DEKTP (cyclic trifunctional), PDP (cyclic bifunctional) and L331 (linear bifunctional). The theoretical work consisted of the development of a comprehensive, generic yet detailed mathematical model for bulk HIPS polymerization using multifunctional initiators. The model predicts the evolution of the main polymerization variables (including conversion, molecular weights, grafting efficiency) as well as the detailed molecular structure of the polymeric species (free polystyrene, residual polybutadiene and graft copolymer), and the melt flow index of the obtained HIPS. The model was adjusted and validated using experimental results, obtaining a good agreement between measured and predicted values. The model was used to theoretically evaluate the effect of the operating conditions on the molecular and physical characteristics of the obtained polymer. It was found that the use of multifunctional initiators leads to high polymerization rates and high molecular weights simultaneously, while promoting the grafting of styrene onto butadiene, generating a microstructure with salami-type morphologies.

INTRODUCTION

High impact polystyrene is a reinforced engineering thermoplastic, which can be industrially produced by bulk polymerization of St in the presence of a rubber (PB or butadiene copolymer). This heterogeneous material consists of a vitreous PS matrix, containing dispersed rubber particles. Said particles contain PS occlusions with different morphologies, the size of which can greatly influence impact resistance [1]. HIPS properties depend not only on the recipe and operating conditions, but also on the technology employed in the production process [2–4].

The industrial bulk process for HIPS production involves four main stages: dissolution, prepolymerization, termination, and devolatilization [5]. In the first stage, the rubber is dissolved into the monomer at relatively low temperatures. The prepolymerization stage consists of the addition of a chemical initiator, under continuous stirring, reaching usually approximately 10-20% conversion. In said stage, the morphology of the material is developed. Termination takes place at higher temperatures, in order to reduce the viscosity and promote the thermal initiation of the monomer. This stage is carried out without stirring, to avoid destruction of the morphology. During the devolatilization stage, the unreacted monomer is removed, under vacuum and at elevated temperatures.

During the prepolymerization, the system is initially homogeneous. However, the thermodynamic incompatibility between PB and PS causes the system to separate into two phases: a continuous, rubber-rich phase and a dispersed, PS-rich phase [6, 7]. The reaction then proceeds with the generation of free PS, and graft copolymer (GC). Towards the end of the prepolymerization stage, a crucial step for the development of morphology takes place, known as phase inversion (PI). After the PI, the morphology remains almost unchanged during the following stages [8]. The PI is basically determined by the volume and viscosity of the phases, the presence of GC, and the stirring conditions [9, 10]. The PI phenomenon has been studied [11–15] but is still poorly understood.

The GC is generated by H-abstraction reactions involving the rubber and a free radical species, resulting in an active site from which a polymer chain can grow. Said radical species can be generated by chemical decomposition of an initiator molecule, which contains a certain number of labile groups, depending on its functionality. As in other industrial free-radical polymerization processes, with the use of monofunctional initiators it is difficult to achieve a good balance between process productivity and product properties [16]. Mixtures of monofunctional initiators with different thermal stabilities have been shown to be a promising alternative in PS production processes [17, 18].

Bifunctional initiators in processes for obtaining HIPS [19–21] have been studied both experimentally and theoretically. It was observed that said initiators allow high productivity and high molecular weights, and can also have an effect on particle morphology [20]. The cyclic trifunctional initiator diethyl ketone triperoxide (DEKTP) has also been experimentally studied in the production of HIPS [22], obtaining products with adequate particle morphology and a good physical properties. It has been

observed that the sequential decomposition of the initiators leads to significant increases in the rate of polymerization, high molecular weights and may introduce branching in the chains leading to improvements in the rheological and processing properties [23].

Most mathematical models for the bulk HIPS process have assumed the reaction system to be homogeneous and allowed to simulate both batch [20, 24] as well as continuous industrial processes [5, 21, 25]. Except in Estenoz et al. [20] where mono- and bifunctional initiators are considered, all the above models are limited to monofunctional initiators. Even though multifunctional initiators are widely used in industrial HIPS processes, there are no available mathematical models to simulate a HIPS polymerization process using linear initiators with functionalities greater than 2 or cyclic multifunctional initiators.

This work is the first attempt to develop a comprehensive mathematical model for the bulk HIPS process using multifunctional initiators. The model allows estimating the evolution of the detailed MWD and molecular structure of the obtained products (free PS, GC, and residual PB). This model can be used to simulate processes using any mono- or multifunctional initiator, either lineal or cyclic. The model is adjusted and validated using new experimental results for the bulk polymerization of St in the presence of PB using different peroxide initiators. The model is also used to theoretically study the use of multifunctional initiators and the effect of process conditions on polymerization rate and product quality.

EXPERIMENTAL WORK

The experimental work consisted on the synthesis and characterization of high impact polystyrenes using three initiators with different functionalities. The selected polymerization temperatures are such that initiator decomposition is mostly sequential [26, 27]. The employed peroxide initiators were:

- Cyclic trifunctional initiator DEKTP (IUPAC Name: 3,3,6,6,9,9-hexaethyl-1,2,4,5,7,8-hexaoxacyclononane);
- Cyclic bifunctional initiator pinacolone diperoxide (PDP) (IUPAC Name: 3,6-ditertbutyl-3,6-dimethyl-1,2,4,5-tetraoxacyclohexane);
- Linear bifunctional initiator Luperox-331M80 (L331) (IUPAC Name: 1,1-Bis(tert-butylperoxy)cyclohexane).

Reagents

Styrene (99%) was provided by Sigma-Aldrich and it was purified by vacuum distillation over sodium before use. 1,1-*Bis*(*tert*-butylperoxy)cyclohexane (Luperox-331M80) was supplied by Arkema and it was used as received. Sodium sulfate (Na_2SO_4, $\geq$99%), petroleum ether (ACS reagent), methanol (99.8%) and tetrahydrofuran (THF, $\geq$99%) were supplied by Sigma-Aldrich and they were used without extra purification. Sulfuric acid (H_2SO_4, 98%) and hydrogen peroxide (H_2O_2, 50%) were purchased from J. T. Baker and used as received. The medium *cis*-PB was provided by Dynastol Elastómeros S.A de C.V., México ($\bar{M}_n$=215 000 g/mol, $\bar{M}_w$=410 000 g/mol). Cyclic initiators DEKTP and PDP were synthesized and characterized as in our previous work [28–30].

TABLE 1. Experimental conditions for HIPS polymerization using multifunctional initiators.

Initiator	$[I_0^{(\phi)}]$ (mol/L)	T_{PP} (°C)
DEKTP	1.56×10^{-3}	120
DEKTP	1.56×10^{-3}	130
PDP	1.56×10^{-3}	110
PDP	1.56×10^{-3}	120
L331	1.56×10^{-3}	110
L331	1.56×10^{-3}	116

Polymerization Reactions

The polymerization reactions consisted of a series of bulk polymerizations of St in the presence of PB, with the main stages of an industrial HIPS process (dissolution, prepolymerization and finishing) using different multifunctional peroxide initiators. In the industrial process, the dissolution and prepolymerization take place in a series of continuously stirred tank reactors, while the finishing takes place in a series of non agitated reactors [5]. The peroxide initiators employed and reaction conditions, including initial initiator concentration of functionality ϕ $[I_0^{(\phi)}]$ and prepolymerization temperature T_{PP} are presented in Table 1.

Dissolution

A metal polymerization reactor was filled with 64 g of PB and 736 g of St and was left under agitation at 70 rpm at room temperature for 12 h until a homogeneous mixture was obtained. The reactor was pressurized with nitrogen at 10 psi.

Prepolymerization

The selected peroxide initiator was added in order to reach a concentration of 1.56×10^{-3} mol/L for all initiators. The reaction mixture was de-gassed and blanketed with nitrogen and the reactor was heated to the selected temperature with a heating coil containing flowing hot oil. The reaction temperature was monitored and controlled using a 4842 PID controller and an air-cooling system in order to keep the temperature at the desired value. Samples were taken along the reaction using a sampling valve located at the bottom of the reaction vessel. In the industrial process, the prepolymerization stage proceeds until phase inversion. For the experimental setup, the prepolymerization time was set to 120 min in order to ensure phase inversion, which was visually verified.

Finishing

After the prepolymerization, five samples were taken from the reaction medium and placed into glass tubes, which are immersed in a bath of deionized water, in order to reach full conversion for 20 h at a finishing temperature T_F of 150°C.

Characterizations

Conversion. The samples taken at the prepolymerization stage were dissolved in 10 times their volume of toluene under agitation at room temperature until full dissolution. The polymer was then precipitated dropwise from methanol, filtered, and dried under vacuum at 50°C until constant weight.

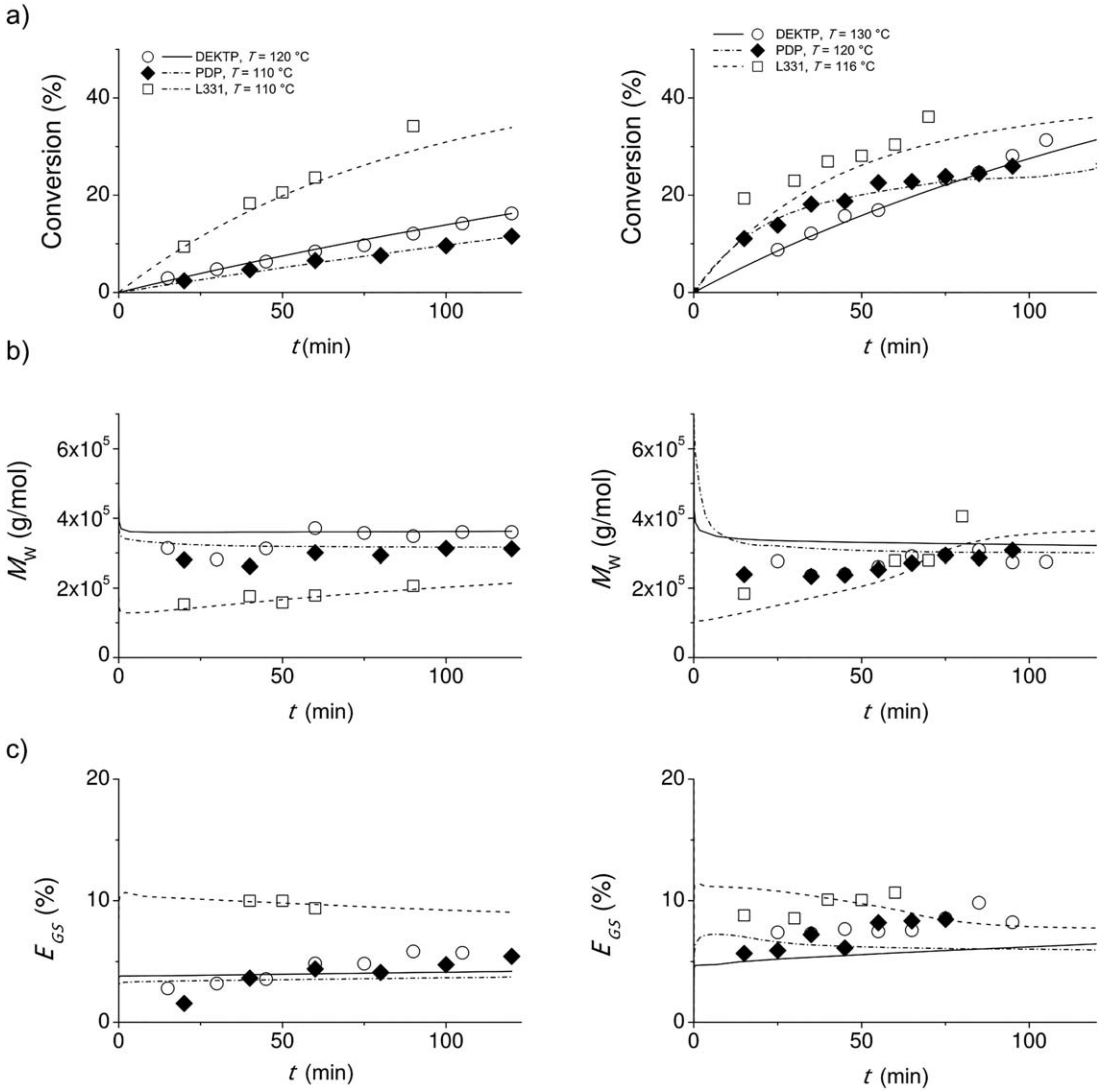

FIG. 1. Time evolution of: (a) monomer conversion; (b) weight-average molecular weight and c) grafting efficiency. On the left, the low temperature cases; on the right, the high temperature ones.

Grafting Efficiency. The grafting efficiency E_{GS} is defined as the ratio between the grafted PS mass and the total PS mass (free and grafted). The free PS was isolated from the other polymer species (PB and GC) using the following solvent extraction technique: 0.5 g of each sample was dissolved in 25 mL of methyl ethyl ketone/dimethylformamide (MEK/DMF; 50% in volume) mixture; under agitation at room temperature until full dissolution. The mixture was then centrifuged at 20,000 rpm at −20°C for 4 h, and an insoluble precipitate and a soluble supernatant were obtained. The free PS from the soluble fraction was precipitated dropwise from methanol, filtered and dried under vacuum at 50°C until constant weight. The precipitate, consisting of the species PB and GC, was isolated from the soluble fraction and dried under vacuum at 50°C until constant weight. The grafted PS was calculated by subtracting the initial PB mass to the PB and GC mass.

Molecular Weights. The molecular weight distribution of the free PS and PB and the corresponding average molecular weights ($\bar{M}_n$ and $\bar{M}_w$) were determined by size exclusion chromatography, using a Hewlett-Packard chromatograph with a series of three PLgel columns (nominal pore size 10^5, 10^4, and 10^3 A). In all cases, a linear molecular weight calibration was obtained. Narrow PS standards were used (polydispersities lower than 1.05 in all cases) and molecular weights in the range of M_p = 162–7,200,000. Tetrahydrofuran (THF, HPLC grade) was used as the eluent at a flow rate of 1 mL/min at 40°C. Injection volume was 100 μL at a concentration of 1 mg/mL using an automatic injector. Samples were analyzed at room temperature.

Morphology. The internal morphology of the obtained polymers was analyzed by Transmission Electron Microscopy (TEM) using a JEOL TEM. The measurements were carried out at 10 kV on sample cuts with a Leica Ultracut ultramicrotome and stained with osmium dioxide during 2 h. The sample cuts were performed at a temperature of −180°C in the ultramicrotome chamber, yielding cuts of no more than 100 nm thickness.

Melt Flow Index. Melt flow index (in g/10 min) of the final polymers was determined as per ASTMD-1238-13, using a Dynisco Ph 800-322-2245 plastomer, a total charge of 5 kg and at a temperature of 200°C.

EXPERIMENTAL RESULTS

The experimental results are presented in Figs. 1 and 2, and Table 2. Figure 1 corresponds to the prepolymerization stage, while Table 2 presents the characteristics of final HIPS samples (at conversion ≈100%). In Fig. 2, the morphologies of the final HIPS samples as observed by TEM are presented.

The evolution of conversion with time during the prepolymerization stage can be observed in Fig. 1. From the slopes of the curves, the rate of polymerization R_p can be estimated. It can be seen that R_p (L331)> R_pDEKTP > R_p (PDP) for the lower temperature experiments. At higher temperatures, it is observed that R_p (PDP)> R_p (DEKTP) up to a prepolymerization time of about 75 min. This could be attributed to the different thermal stability of the peroxide groups of the initiators. Note that the R_p are not always determined at the same prepolymerization temperature.

The highest polymerization rates for L331 can be attributed to a higher decomposition rate of the peroxide, as well as higher initiator efficiency. The decompositions of peroxide groups in PDP appears to be more thermally activated than that of peroxide groups in DEKTP, which would explain the observed differences in relative R_p behavior at lower or higher temperatures.

As regards the molecular weights, it can be seen that in the case of the cyclic initiators DEKTP and PDP, molecular weights are approximately constant throughout the prepolymerization reaction, both at higher and lower temperatures. At lower temperatures, molecular weights obtained with L331 are slightly lower than those obtained using the cyclic initiators, in accordance with a higher decomposition rate of peroxide groups in L331. However, for the experiment at higher temperature, it can be observed that molecular weights increase along the reaction. At the end of the prepolymerization stage, average molecular weights obtained with L331 are higher than those obtained with cyclic initiators.

The behaviors observed for the evolution of conversion and free PS average molecular weights attributed to the higher stability of the cyclic initiators DEKTP and PDP are consistent with what was found in our previous work with respect to the different decomposition rates of these multifunctional initiators [30].

As regards the grafting efficiency, it should be noted that this variable is expected to have a large uncertainty due to the experimental technique employed for its determination [20]. The differences in experimental values are relatively small, although it can generally be seen that E_{GS}(L331) > E_{GS} (PDP) > E_{GS} (DEKTP). This can be attributed to a higher rate of H-abstraction reactions by initiator radicals, which generate grafting points in the PB chains. An increase in prepolymerization temperature promotes higher grafting efficiencies for the cyclic initiators DEKTP and PDP.

The different values for grafting efficiencies and number of grafting points during prepolymerization are also related to the differences in the observed morphologies for the final products

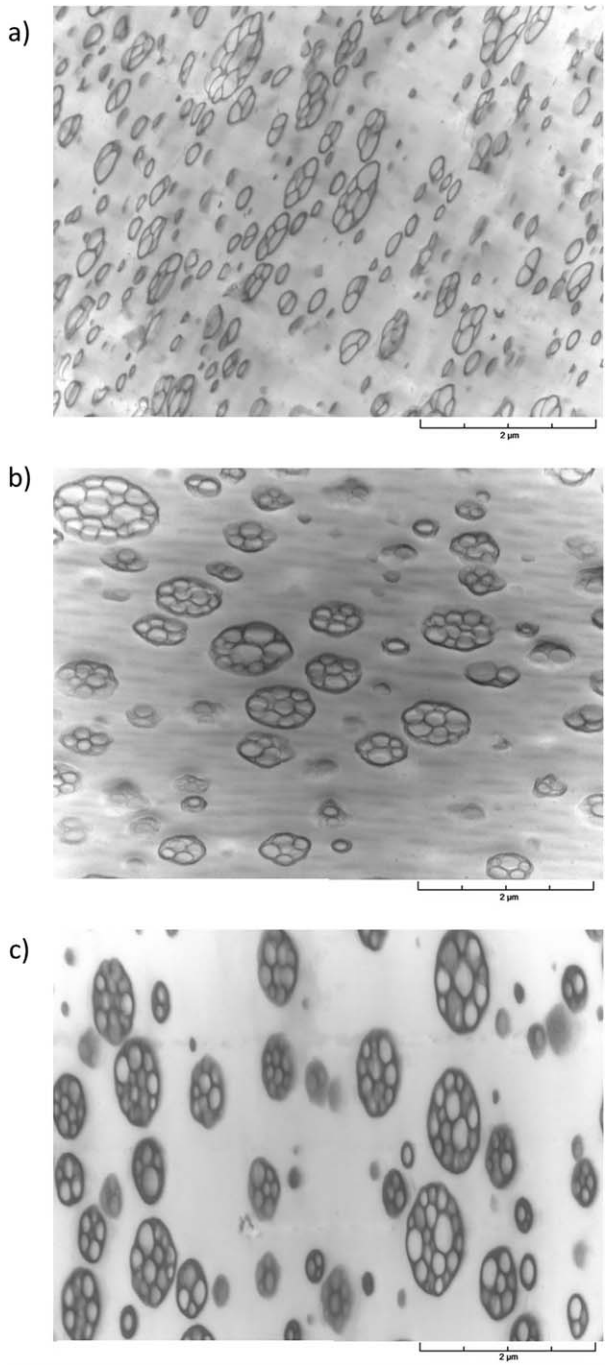

FIG. 2. HIPS final morphologies as observed by TEM, for the (a) L331, (b) PDP, and (c) DEKTP initiators.

of Fig. 2. It can be observed that the product obtained with L331 presents a larger number of smaller particles, of an average diameter of approximately 290 nm and core–shell morphologies. In contrast, the product obtained with PDP and DEKTP presents a smaller number of larger particles, with average diameters of approximately 510 and 870 nm respectively, and salami morphologies.

With respect to the final properties of the HIPS samples in Table 2, it can be seen that the products synthesized with the cyclic initiators PDP and DEKTP present similar values for

TABLE 2. Final properties of the synthesized HIPS materials. Theoretical predictions are indicated in parenthesis.

Initiator	T_{PP} (°C)	T_F (°C)	$\bar{M}_{w,PS}\times10^{-5}$ (g/mol)	E_{GS} (%)	MFI (g/10 min)
DEKTP	120	150	1.79 (1.76)	17 (15)	18 (10.7)
PDP	110	150	1.75 (1.83)	18 (17)	12 (9.2)
L331	116	150	3.00 (2.75)	20 (19)	2.0 (3.5)

$\bar{M}_{w,PS}$, $E_{GS,}$ and MFI. Initiation by DEKTP produces a product of higher molecular weight than the product obtained with PDP, in accordance with the values of the molecular weights during the prepolymerization stage. Additionally, the higher $\bar{M}_{w,PS}$ and E_{GS} values observed in the case of L331 are consistent with the differences in values observed during the prepolymerization stage. The experimental results for the product synthesized with DEKTP show an unexpected behavior in the high MFI value, which is inconsistent with the higher molecular weight. This result can be attributed to the possible presence of small amounts of monomer in the melt.

TABLE 3. Proposed kinetic mechanism.

Initiation ($\phi=1,2,3; i<\phi; j=0,1,\ldots$)

Thermal initiation

$3\mathrm{St}\xrightarrow{k_{i0}}2S_1{}^{\cdot(0)}$

Chemical initiation

$I^{(\phi)}\xrightarrow{\phi k_{d1}}\cdot I^{\cdot(\phi-1)}$

$\bar{I}^{(\phi)}\xrightarrow{\phi k_{d1}}\bar{I}^{\cdot(i)}$

$\cdot I^{\cdot(i)}+\mathrm{St}\xrightarrow{2k_{i1}}\cdot S_1{}^{\cdot(i)}$

$I^{\cdot(i)}+\mathrm{St}\xrightarrow{k_{i1}}S_1{}^{\cdot(i)}$

$\cdot I^{\cdot(i)}+P^{(j)}\xrightarrow{2k_{i2}}P_0{}^{\cdot(j)}+I^{\cdot(i)}$

$I^{\cdot(i)}+P^{(j)}\xrightarrow{k_{i2}}P_0{}^{\cdot(j)}+\bar{I}^{(i)}$

Propagation ($n=1,2,3,\ldots; i=0,1,2\ldots$)

$S_n{}^{\cdot(i)}+\mathrm{St}\xrightarrow{k_p}S_{n+1}{}^{\cdot(i)}$

$\cdot S_n{}^{\cdot(i)}+\mathrm{St}\xrightarrow{2k_p}\cdot S_{n+1}{}^{\cdot(i)}$

$P_0{}^{\cdot(i)}+\mathrm{St}\xrightarrow{k_p}P_1{}^{\cdot(i)}$

$P_n{}^{\cdot(i)}+\mathrm{St}\xrightarrow{k_p}P_{n+1}{}^{\cdot(i)}$

Transfer to monomer ($n=1,2,3,\ldots; i=0,1,2\ldots$)

$S_n{}^{\cdot(i)}+\mathrm{St}\xrightarrow{k_{fM}}S_n{}^{(i)}+S_1{}^{\cdot(0)}$

$\cdot S_n{}^{\cdot(i)}+\mathrm{St}\xrightarrow{2k_{fM}}S_n{}^{\cdot(i)}+S_1{}^{\cdot(0)}$

$P_0{}^{\cdot(i)}+\mathrm{St}\xrightarrow{k'_{fM}}P^{(i)}+S_1{}^{\cdot(0)}$

$P_n{}^{\cdot(i)}+\mathrm{St}\xrightarrow{k_{fM}}P^{(i)}+S_1{}^{\cdot(0)}$

Transfer to rubber ($n=1,2,3,\ldots; i,j=0,1,2\ldots$)

$S_n{}^{\cdot(i)}+P^{(j)}\xrightarrow{k_{fG}}S_n{}^{(i)}+P_0{}^{\cdot(j)}$

$\cdot S_n{}^{\cdot(i)}+P^{(j)}\xrightarrow{2k_{fG}}S_n{}^{\cdot(i)}+P_0{}^{\cdot(j)}$

$P_0{}^{\cdot(i)}+P^{(j)}\xrightarrow{k_{fG}}P^{(i)}+P_0{}^{\cdot(j)}$

$P_n{}^{\cdot(i)}+P^{(j)}\xrightarrow{k_{fG}}P^{(i)}+P_0{}^{\cdot(j)}$

Reinitiation ($n=2,3,\ldots; m=1,2,\ldots,n-1; i=1,2\ldots; j=0,1,\ldots,i-1$)

$S_n{}^{(i)}\xrightarrow{ik_{dp}}S_{n-m}{}^{\cdot(i-j)}+S_m{}^{(j-1)}.$

$P^{(i)}\xrightarrow{ik_{dp}}P_{n-m}{}^{\cdot(i-j)}+S_m{}^{(j-1)}.$

Termination by combination ($n,m=1,2,3\ldots; i,j=0,1,2\ldots$)

$\cdot S_n{}^{\cdot(i)}+\cdot S_m{}^{\cdot(j)}\xrightarrow{4k_{tc}}\cdot S_{n+m}{}^{(i+j)}.$

$\cdot S_n{}^{\cdot(i)}+S_m{}^{\cdot(j)}\xrightarrow{2k_{tc}}S_{n+m}{}^{(i+j)}.$

$S_n{}^{\cdot(i)}+S_m{}^{\cdot(j)}\xrightarrow{k_{tc}}S_{n+m}{}^{(i+j)}$

$P_0{}^{\cdot(i)}+P_0{}^{\cdot(j)}\xrightarrow{k'_{tc}}P^{(i+j)}$

$P_0{}^{\cdot(i)}+P_m{}^{\cdot(j)}\xrightarrow{k_{tc}}P^{(i+j)}$

$P_n{}^{\cdot(i)}+P_m{}^{\cdot(j)}\xrightarrow{k_{tc}}P^{(i+j)}$

$P_n{}^{\cdot(i)}+\cdot S_m{}^{\cdot(j)}+\xrightarrow{2k''_{tc}}P_{n+m}^{(i+j)}.$

$P_0{}^{\cdot(i)}+S_m{}^{\cdot(j)}+\xrightarrow{k''_{tc}}P^{(i+j)}$

$P_n{}^{\cdot(i)}+S_m{}^{\cdot(j)}+\xrightarrow{k''_{tc}}P^{(i+j)}$

MATHEMATICAL MODEL

Pseudo-Homogeneous Polymerization Model

The mathematical model is based on the kinetic mechanism presented in Table 3, which includes initiation via a symmetrical cyclic or linear multifunctional initiator, thermal initiation, propagation, transfer to the monomer, transfer to the rubber, termination by combination, and re-initiation. The following nomenclature was adopted:

$\bar{\mathrm{I}}^{(\phi)}$	Cyclic multifunctional initiator with ϕ undecomposed peroxide groups.
$\bar{\mathrm{I}}^{(\phi)}$	Linear multifunctional initiator with ϕ undecomposed peroxide groups.
$\cdot\mathrm{I}^{\cdot(i)}$	Initiator diradical with i undecomposed peroxide groups.
$\mathrm{I}^{\cdot(i)}$	Initiator monoradical with i undecomposed peroxide groups.
$\cdot S_1{}^{\cdot(i)}$	Monomer diradical with i undecomposed peroxide groups.
$S_1{}^{\cdot(i)}$	Monomer monoradical with i undecomposed peroxide groups.
$S_n{}^{\cdot(i)}$	PS monoradical of chain length n containing i undecomposed peroxide groups.
$\cdot\mathrm{S}_n{}^{\cdot(i)}$	PS diradical of chain length n containing i undecomposed peroxide groups.
$S_n{}^{(i)}$	Polymer with n repetitive units of St and i undecomposed peroxide groups.
$P^{(i)}$	Copolymer with i undecomposed peroxide groups in the grafted chain.
$P_0{}^{\cdot(i)}$	Primary Radical produced by attack to a butadiene repetitive unit (B) present in the residual PB or the $P^{(i)}$.
$P_n{}^{\cdot(i)}$	Copolymer radical with i undecomposed peroxide groups and n repetitive units of St in the active branch.

The following was considered: (i) at the temperatures employed, the initiators decompositions are due exclusively to sequential decomposition [16, 26, 27]; (ii) intramolecular termination is negligible [20]; (iii) disproportion termination is negligible [31]; (iv) all peroxide groups present in the initiator and in the accumulated homo- and copolymers exhibit the same thermal stability [20]; (v) because of the short lifetime of radicals, the decomposition of undecomposed peroxide groups does not occur in radical molecules [20]; (vi) propagation and transfer reactions are unaffected by the chain length or conversion [20]; (vii) degradation reactions are negligible [32].

Assuming a homogeneous bulk polymerization [20], a mathematical model was developed from the kinetic mechanism detailed in Table 3. The model consists of a set of nonlinear differential equations, which are derived from the mass balances for the reacting species (see Appendices A and B), including the living radical species, dead, and temporarily dead polymer and copolymer species for all kinetic chain lengths and number of undecomposed peroxide groups.

TABLE 4. Adopted kinetic parameters.

Kinetic parameter	Units	Arrhenius expression	References
k_{d1}, k_{dp} (DEKTP)	$[s^{-1}]$	$3.4\times10^{42}e^{-43548/T}$	Adjusted in this work
k_{d1}, k_{dp} (PDP)	$[s^{-1}]$	$4.1\times10^{61}e^{-58622/T}$	Adjusted in this work
k_{d1}, k_{dp} (L331)	$[s^{-1}]$	$1.9\times10^{20}e^{-21034/T}$	Adjusted in this work
f_1, f_2 (DEKTP)		$0.034T-12.7$	Adjusted in this work
f_1, f_2 (PDP)		$0.017T-6.40$	Adjusted in this work
f_1, f_2 (L331)		$0.0073T-1.96$	Adjusted in this work
k_{i0}	$\left[\frac{L^2}{mol^2 s}\right]$	$1.1\times10^{5}e^{-13810/T}$	Casis et al. [35]
k_{i1}, k_p	$\left[\frac{L}{mol\ s}\right]$	$1.051\times10^{7}e^{-7067/RT}$	Estenoz et al. [20]
k_{i2} (DEKTP)	$\left[\frac{L}{mol\ s}\right]$	$7.6\times10^{4}e^{-2115/T}$	Adjusted in this work
k_{i2} (PDP)	$\left[\frac{L}{mol\ s}\right]$	$8.3\times10^{8}e^{-6103/T}$	Adjusted in this work
k_{i2} (L331)	$\left[\frac{L}{mol\ s}\right]$	$1.8\times10^{3}e^{-492/T}$	Adjusted in this work
k_{fM}, k'_{fM}	$\left[\frac{L}{mol\ s}\right]$	$3.2\times10^{12}e^{-11698/T}$	Adjusted in this work
$k_{tc}, k'_{tc}, k''_{tc}$	$\left[\frac{L}{mol\ s}\right]$	$1.686\times10^{9}e^{-(844/T)-2(C_1x+C_2x^2+C_3x^3)}$ [a]	Casis et al. [35]

[a] $C_1=2.57-0.00505T$; $C_2=9.56-0.0176T$; $C_3=-3.03+0.00785T$, with x monomer conversion.

The mathematical model consists of three modules:

- The Basic module (Appendix A), which allows the prediction of global chemical species evolution along the reaction (monomer, initiators, total radical species, unreacted B units, grafting efficiency).
- The Distributions module (Appendix B), which simulates the evolution of all chemical species, characterized by their chain length and number of undecomposed peroxide groups. The equations estimate the evolution of the complete MWD of each radical and polymer species, including free PS and residual PB and GC. In order to consider the effect of re-initiation reactions in the MWDs, PS chains were assumed to have uniformly distributed peroxide groups. A random-chain scission can be simulated with a uniformly distributed random variable. The uniform peroxide group distribution hypothesis is expected to be valid for cyclic initiators and for linear initiators with functionalities greater than two [30].
- The Melt flow index module (Appendix C), which estimates the MFI of the obtained polymer by considering the mass and momentum balances in a plastometer [25] The MFI module inputs are the plastomer characteristics—dimensions and operating conditions—as well as the final HIPS characteristics.

The proposed model does not include an energy balance. However, nonisothermal reactions can be simulated through the use of standard or modified Arrhenius expressions for the kinetic constants [20, 32]. When a temperature profile is imposed, the reactor cooling/heating system is considered ideal, in the sense that it is capable of exactly following said profile. The gel effect was indirectly considered by appropriately reducing the value of the termination kinetic coefficient with increasing conversion, using an empirical free-volume based expression [32].

For the Basic module, Eqs. (A.1)–(A.6), (A.8), (A.9), (A.19), (A.23)–(A.29) must be simultaneously solved. The Distributions module is then solved using the results from the Basic module. Finally, the MFI module is solved using the weight average molecular weights calculated with the Distribution module. The Basic Module is solved by a standard stiff differential equation numerical method based on a second-order modified Rosenbrock formula, programmed in MATLAB v. 8.3. In the Distributions module, a large number of equations (more than 500,000) must be integrated. For this reason, an explicit forward Euler method was used, with the time intervals obtained from resolution of the basic module. The MFI module is solved using a Newton–Raphson method for solving a system of nonlinear algebraic equations. A typical simulation requires less than 1 s for the Basic module, about 5 min for the Distributions module and less than 1 s for the MFI module with an Intel Core i5 based processor at 2.40 GHz. For the copolymer bivariate distribution, a very large number of differential equations must be solved, involving large variables in order to consider every possible number of St and B units. For this reason, a cruder numerical method was employed, considering for each time interval, the instantaneous chain length distribution (CLD) of the grafted St and number of grafting points estimated from the Basic module. It was assumed that the instantaneous CLD of the grafted PS chains is equal to the CLD the free PS [20].

Model parameter adjustment was sequential and consisted of three steps, using least-squares optimization algorithms. Firstly, k_{d1}, k_{dp}, f_1, and f_2 for each initiator were adjusted with the conversion data. Since all peroxide groups are assumed to have the thermal stability, $k_{dp} = k_{d1}$ and it was assumed that $f_1 = f_2$. Secondly, k_{fM} was adjusted with the average molecular weight data. Thirdly, k_{i2} and k_{fG} were adjusted with the experimental grafting efficiency data. The obtained values for the decomposition constants are in accordance with what has been reported for the decomposition rates of organic peroxides [33], and the values for the other constants are within the expected range reported in the literature [34]. All other values for the kinetic parameters were taken from the literature [32]. Model parameters are presented in Table 3.

Simulation Results

It was found that f_1k_{d1}(L331) $> f_1k_{d1}$(PDP) $> f_1k_{d1}$(DEKTP), which is in accordance to what was found in our previous works for St homopolymerization. In addition, it was found that k_{i2}(L331) $>$ (PDP) $>k_{i2}$(DEKTP), indicating that the

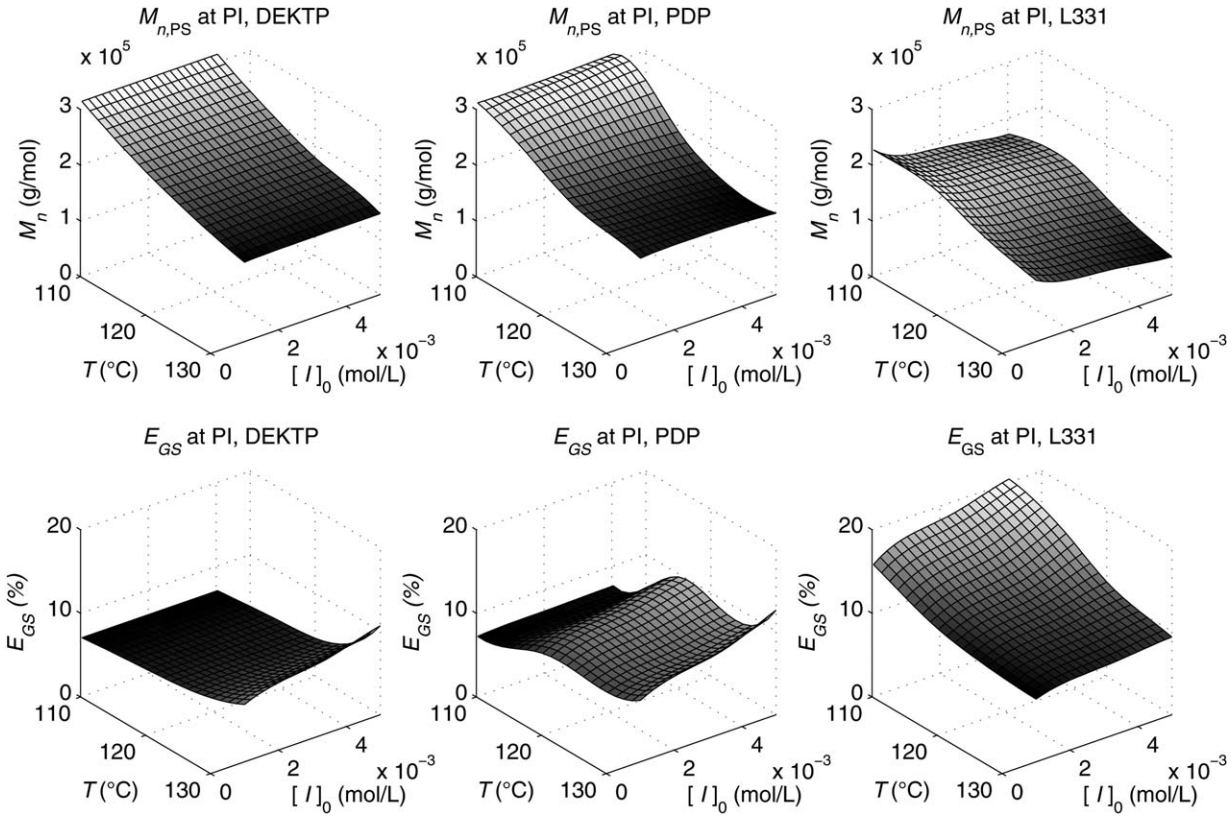

FIG. 3. Theoretical simulations for HIPS Polymerization using multifunctional initiators.

bifunctional linear initiator generates a higher number of grafting points at a given temperature. This result is in agreement with the lower grafting efficiencies observed for DEKTP and PDP compared to L331 and with the different morphologies observed in the final products.

Simulation results are compared to experimental results in Fig. 1 and Table 2. In general, a good agreement between experimental and predicted values is observed.

The predicted evolution of average molecular weights during the prepolymerization stage shows an increase in the values for linear initiator L331, while the molecular weights remain approximately constant for cyclic initiators PDP and DEKTP. This behavior is in agreement with the results from our previous works. As the temperature is increased to 150°C for the finishing stage, the values of average molecular weights decrease.

Other simulation results using the model are presented in Fig. 3. As shown, the model can be used to obtain smooth surfaces given by the values of $\bar{M}_n$ and E_{GS} at a given instant during the polymerization, as a function $[I^{(\phi)}]_0$ and T_{PP}. Given that the characteristics of the final product are greatly determined at the

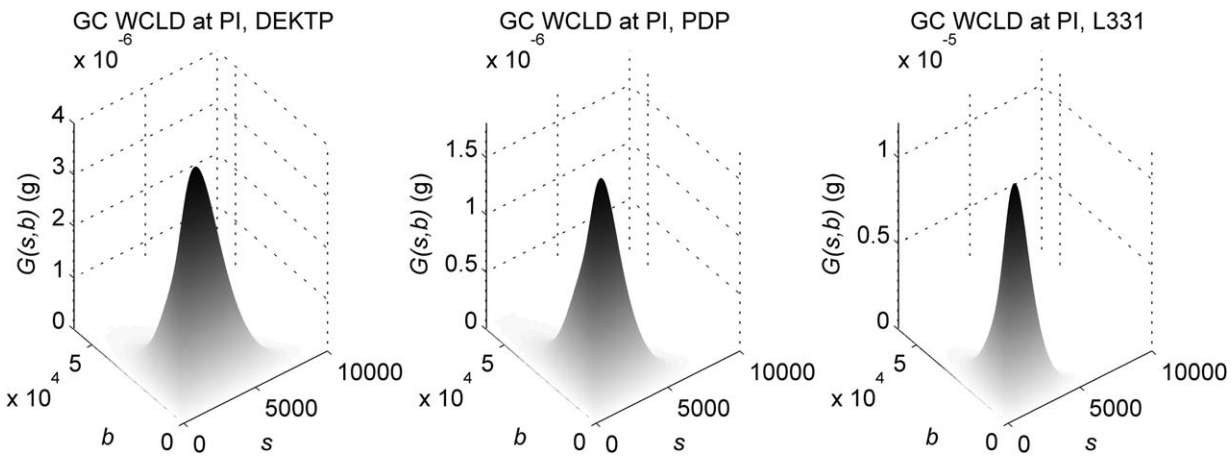

FIG. 4. Weight-chain length distributions at the phase inversion point for each initiator.

TABLE 5. Copolymer average molecular weights, chemical composition, and number of grafted branches at the phase inversion point.

Initiator	T_{PP} (°C)	T_F (°C)	$\bar{M}_{n,C}$ (g/mol)	$\bar{M}_{w,C}$ (g/mol)	$\bar{\omega}_{St}$	J (#/molecule)
DEKTP	120	150	196325	370403	0.49	0.64
PDP	110	150	206747	401301	0.50	0.64
L331	116	150	173727	315098	0.41	0.63

PI point, said point was chosen to evaluate the number average molecular weight of the free PS and the grafting efficiency. To estimate the PI point, the evolution of the volumes of hypothetical PS- and PB-rich phases was calculated using the results from the model. It was assumed that the PI point is the point at which the volumes of both phases is equal [35] The value of conversion at which PI occurs in the simulated conditions is found to be approximately 12%, within the range reported in the literature [8].

For all initiators, it can be seen that increasing the prepolymerization temperature for a given initial concentration results in lower molecular weights at the PI, as expected. The effect of the initial initiator concentration at a given temperature depends on the choice of the initiator. For the cyclic peroxides DEKTP and PDP, it can be seen that $\bar{M}_{n,PS}$ at the PI point is very slightly dependent on initiator concentration. This has been experimentally verified in previous works [22] and is related to the higher stability and lower decomposition rate of the cyclic initiators. In the case of L331, molecular weights decrease with increasing initiator concentration, due to the higher decomposition rate which generates a higher number of active sites.

As regards grafting efficiencies at the PI point, it can be seen that cyclic initiators provide lower values than the linear initiator, indicating a lower selectivity toward grafting reactions with this type of initiators, as previously reported [22]. As expected, increasing initiator concentration increases the grafting efficiency. The effect of the prepolymerization temperature depends on the initiator: for cyclic initiators, an increase in grafting efficiency with increasing temperature is observed.

If the molecular structure at the PI point was correlated to the final product morphologies, this model could be used to find the optimum conditions of the prepolymerization stage (T_{PP}, $[I^{(\phi)}]_0$) to obtain a product with a prespecified morphology. Analogously, the model can also be used to obtain the optimum temperature profile during the finishing stage in order to obtain a pre-specified MFI. Simulations such as the ones shown in Fig. 3 are a first step towards model inversion.

The model can also be used to estimate the molecular structure of the graft copolymer at the PI point. Figure 4 shows the detailed weight chain length distributions at the PI point obtained using the multifunctional initiators at a given prepolymerization temperature T_{PP} and an initial concentration of 1.56×10^{-3} mol/L.

The average molecular characteristics of the graft copolymer (average molecular weights, average St mass fraction $\bar{\omega}_{St}$ and average number of grafted St branches per reacted PB molecule J as estimated by the model are presented in Table 5. As expected, it can be observed the cyclic initiators provide higher copolymer average molecular weights. The chemical compositions and average number of St branches are within the ranges reported in previous works [20].

CONCLUSIONS

A mathematical model for the bulk polymerization of styrene in the presence of polybutadiene using multifunctional initiators was presented. The model simulates the evolution of all the chemical species in the reaction system, consisting of a prepolymerization stage and a finishing stage and predicts the melt flow index of the obtained HIPS.

The model was adjusted and validated using the experimental data from batch HIPS polymerizations using initiators DEKTP, PDP, and L331. The kinetic mechanism includes the reinitiation reactions due to undecomposed peroxide groups within the polystyrene chains and the derived model can be used to evaluate the detailed molecular structure of all polymer species, including free PS, residual PB and graft copolymer. Theoretical and experimental results indicate that the decomposition rates of the initiator functional groups are key variables in determining the characteristics of the final products, namely average molecular weights, grafting efficiency and particle morphology.

The model can be used to evaluate the influence of the recipe and operating conditions on the molecular and physical characteristics of the obtained polymer and find the conditions for synthesizing a polymer with a set of pre-specified properties.

REFERENCES

1. S.Y. Hobbs, *Polym. Eng. Sci.*, **26**, 1 (1986).
2. G. Dagli, A.S. Argon, and R.E. Cohen, *Polymer*, **36**, 11 (1995).
3. S. Joseph and S. Thomas, *Eur. Polym. J.*, **39**, 1 (2003).
4. G. Morales, R. Díaz de León, and P. Acuña, *Polym. Eng. Sci.* doi: 10.1002/pen (2006).
5. D.A. Estenoz and G.R. Meira, *AIChE J.*, **44**, 2 (1998).
6. W.A. Ludwico and S.L. Rosen, *J. Appl. Polym. Sci.*, **19**, 3 (1975).
7. M. Fischer and G.P. Hellmann, *Macromolecules*, **29**, 7 (1996).
8. G. Soto, E. Nava, M. Rosas, M. Fuenmayor, I.M. Gonza, G.R. Meira, and H.M. Oliva, *J. Appl. Polym. Sci.*, **91**, (2004).
9. G.F. Freeguard and M. Karmarkar, *J. Appl. Polym. Sci.*, **15**, 7 (1971).
10. S. Zhiqiang, Y. Huigen, and P. Zuren, *J. Appl. Polym. Sci.*, **32**, 2 (1986).
11. J.Y. Park and O.O. Park, *Adv. Polym. Technol.*, **15**, (1996).
12. G.P. Leal and J.M. Asua, *Polymer (Guildf)*, **50**, 1 (2009).
13. R. D. de León and G. Morales, *Pol. Eng. & Sci.*, **50**, 373 (2010). doi:10.1002/pen
14. M. Vonka and J. Kosek, *Chem. Eng. J.*, **207–208**, 895 (2012).
15. F. Soriano-Corral, G. Morales, P. Acuña, E. Díaz-Barriga, B. Arellano, C. Vargas, and O. De la Paz, *Macromol. Symp.*, **325–326**, 1 (2013).
16. M.A. Villalobos, A.E. Hamielec, and P.E. Wood, *J. Appl. Polym. Sci.*, **42**, (1991).
17. K.J. Kim, K.Y. Choi, and J.C. Alexander, *Polym. Eng. Sci.*, **30**, 5 (1990).
18. K.J. Kim, K.Y. Choi, and J.C. Alexander, *Polym. Eng. Sci.*, **31**, 5 (1991).
19. I.M. Gonzalez, G.R. Meira, and H.M. Oliva, *J. Appl. Polym. Sci.*, **59**, 3000 (1996).
20. D.A. Estenoz, E. Valdez, H.M. Oliva, and G.R. Meira, *J. Appl. Polym. Sci.*, **59**, 5 (1996).

21. R. López-Negrete de la Fuente, J. Lopez-Rubio, A. Flores-Tlacuahuac, and E. Saldívar-Guerra, *Indus. Eng. Chem. Res.*, **45**, 5 (2006).
22. P. Acuña, G. Morales, and R. Díaz de León, *J. Appl. Polym. Sci.*, **114**, (2009).
23. Scorah, M. J. Experimental and modeling investigation of a novel tetrafunctional initiator in free radical polymerization. Doctoral Thesis, University of Waterloo (2005).
24. F.M. Peng, *J. Appl. Polym. Sci.*, **40**, (1990).
25. C.V. Luciani, D.A. Estenoz, G.R. Meira, and H.M. Oliva, *Indus. Eng. Chem. Res.*, **44**, 22 (2005).
26. Cerna Cortez, J.R. (2002). Uso de peróxidos cíclicos multifuncionales como iniciadores de la polimerización.
27. Castañeda Facio, A.V. (2007) Estudio de la Descomposición Térmica del Diperóxido de Pinacolona: Formación de Oligómeros y Polímeros a base de Estireno con estructura definida (2007).
28. E. Berkenwald, C. Spies, J.R. Cerna Cortez, G. Morales, and D.A. Estenoz, *J. Appl. Polym. Sci*, **128**, 1 (2013).
29. E. Berkenwald, C. Spies, G. Morales, and D.A. Estenoz, *Polym. Eng. Sci*, **55**, 1 (2015).
30. E. Berkenwald, L. Laganá, P. Acuña, G. Morales, and D. Estenoz, *Int. J. Chem. React. Eng.*, **14**, 1 (2016).
31. J.H. Duerksen and A.E. Hamielec, *J. Polym. Sci. C: Polym. Symp.*, **25**, 1 (2007).
32. A.W. Hui and A.E. Hamielec, *J. Appl. Polym. Sci.*, **16**, 3 (1972).
33. J.R. Cerna, G. Morales, G.N. Eyler, and A.I. Cañizo, *J. Appl. Polym. Sci.*, **83**, 1 (2002).
34. T. Meyer, and J. Keurentjes, (Eds.), Handbook of Polymer Reaction Engineering, Wiley (2005).
35. N. Casis, D.A. Estenoz, L.M. Gugliotta, H.M. Oliva, and G.R. Meira, *J. Appl. Polym. Sci.*, **99**, 6 (2006).
36. P.J.D. Carreau, D.C. Kee, and R.P. Chhabra, *AIChE J.*, **45**, 8 (1999).
37. B. Elbirli and M.T. Shaw, *J. Rheol. (N. Y. N. Y)*, **22**, 5 (1978).
38. J.Z. Liang, and J.N. Ness, *Polymer Testing*, **16**, 403 (1997).
39. R.L. Kruse, *J. Rheol. (N. Y. N. Y)*, **24**, 6 (1980).
40. K.C. Seavey, Y.A. Liu, N.P. Khare, T. Bremner, and C.C. Chen, *Indus. Eng. Chem. Res*, **42**, 21 (2003).
41. D.C. Rohlfing, and J. Janzen, *Ann. Tech. Conf.- Soc. Plast. Eng.*, 1010-1014 (1997).

APPENDIX A: BASIC MODULE

Balances for the Nonpolymeric Reagents and Products

Multifunctional Initiators ($\phi=1,2,3$).

$$\frac{d}{dt}\left([I^{(\phi)}]V\right)=-\phi k_{d1}[I^{(\phi)}]V \tag{A.1}$$

$$\frac{d}{dt}\left([\bar{I}^{(\phi)}]V\right)=-\phi k_{d1}[\bar{I}^{(\phi)}]V \tag{A.2}$$

Secondary Initiator Species.

$$\frac{d}{dt}\left([\bar{I}^{(i)}]V\right)=-ik_{d1}[\bar{I}^{(i)}]V+(1-f_1)\sum_{j=i+1}^{\phi}jk_{d1}\left([I^{(j)}]+[\bar{I}^{(j)}]\right)V \tag{A.3}$$

Monomer. Assuming the long chain hypothesis, by which propagation is the only monomer-consuming reaction:

$$\frac{d}{dt}([\mathrm{St}]V)=-R_\mathrm{p}V=-k_\mathrm{p}[\mathrm{St}]([R\cdot]+2[\cdot R\cdot])V \tag{A.4}$$

where R_p is the global St polymerization rate, and

$$[R\cdot]=[S\cdot]+[P\cdot]=\sum_{i=0}^{\infty}\sum_{n=1}^{\infty}[S_n{}^{\cdot(i)}]+\sum_{i=0}^{\infty}\sum_{n=1}^{\infty}[P_n{}^{\cdot(i)}] \tag{A.5a}$$

$$[\cdot R\cdot]=\sum_{i=0}^{\infty}\sum_{n=1}^{\infty}[\cdot S_n{}^{\cdot(i)}] \tag{A.5b}$$

represent the total concentrations of mono- and diradicals respectively. In (A.5), an S species is a PS homoradical, and a P species is a PB or copolymer radical.

Unreacted *B* Units. Let us represent with B^* an unreacted B unit in the copolymer or in the initial (or purely crosslinked) PB. When a P molecule is attacked, a B^* unit is consumed, and a B^* unit is generated in transfer reactions of a $P_0\cdot$ radical, thus

$$\frac{d}{dt}([B^*]V)=-\left\{k_{i2}\quad 2\sum_{j=0}^{\phi-1}[\cdot I^{\cdot(j)}]+\sum_{j=0}^{\phi-1}[I^{\cdot(j)}]\right)+k_\mathrm{fG}([R\cdot]+2[\cdot R\cdot])\Bigg\}$$
$$[B^*]V+k_\mathrm{fM}[\mathrm{St}][P_0\cdot]V$$

with

$$[P_0\cdot]=\sum_{i=0}^{\infty}[P_0{}^{\cdot(i)}] \tag{A.7}$$

Radical Species ($i=0,1,\ldots;n=2,3,\ldots$). Consider the mass balances of all free radical appearing in the global kinetics. Such balances provide:

$$\frac{d}{dt}\left([\cdot I^{\cdot(i)}]V\right)=f_1(i+1)k_{d1}[I^{(i+1)}]V-2\left(k_{p1}[\mathrm{St}]+k_{i2}[B^*]\right)[\cdot I^{\cdot(i)}]V \tag{A.8}$$

$$\frac{d}{dt}\left([I^{\cdot(i)}]V\right)=\sum_{j=i+1}^{\phi}p_j(i)f_1jk_{d1}[\bar{I}^{(j)}]V$$
$$+2k_{i2}[B^*][\cdot I^{\cdot(j)}]V-(k_{i1}[\mathrm{St}]+k_{i2}[B^*])[I^{\cdot(i)}]V \tag{A.9}$$

where $p_i(j)$ is the probability that the decomposition of the initiator of functionality j generates a monoradical with i undecomposed peroxide groups.

For PS homoradicals,

$$\frac{d}{dt}\left([\cdot S_1\cdot^{(i)}]V\right)=2k_{i1}[\cdot I\cdot^{(i)}][\mathrm{St}]V$$
$$-2\left(k_\mathrm{p}[\mathrm{St}]+k_\mathrm{fM}[\mathrm{St}]+k_\mathrm{fG}[B^*]+k_\mathrm{tc}([R\cdot]+2[\cdot R\cdot])+k''_\mathrm{tc}[P_0\cdot]\right)[\cdot S_1\cdot^{(i)}]V \tag{A.10}$$

$$\frac{d}{dt}\left([S_1\cdot^{(i)}]V\right)=\left\{k_{i1}[I\cdot^{(i)}][\mathrm{St}]+\right\}V++\delta_{i0}\left(2k_{i0}[\mathrm{St}]^3+k_\mathrm{fM}([R\cdot]+2[\cdot R\cdot])[\mathrm{St}]\right)V$$
$$-\left(k_\mathrm{p}[\mathrm{St}]+k_\mathrm{fM}[\mathrm{St}]+k_\mathrm{fG}[B^*]+k_\mathrm{tc}([R\cdot]+2[\cdot R\cdot])+k''_\mathrm{tc}[P_0\cdot]\right)[S_1\cdot^{(i)}]V \tag{A.11}$$

where δ_{i0} is the Kronecker delta.

$$\frac{d}{dt}\left([\cdot S_n\cdot^{(i)}]V\right)=2k_\mathrm{p}[\mathrm{St}]\left([\cdot S_{n-1}\cdot^{(i)}]-[\cdot S_n\cdot^{(i)}]\right)V$$
$$-2\left(k_\mathrm{fM}[\mathrm{St}]+k_\mathrm{fG}[B^*]+k_\mathrm{tc}([R\cdot]+2[\cdot R\cdot])+k''_\mathrm{tc}[P_0\cdot]\right)[\cdot S_n\cdot^{(i)}]V$$
$$+2k_\mathrm{tc}\sum_{j=0}^{i}\sum_{m=1}^{n-1}[\cdot S_{n-m}\cdot^{(i-j)}][\cdot S_m\cdot^{(j)}]V \tag{A.12}$$

$$\frac{d}{dt}\left([S_n\cdot^{(i)}]V\right)=\left(k_p\left([S_{n-1}\cdot^{(i)}]-[S_n\cdot^{(i)}]\right)+2k_\mathrm{fM}[\cdot S_n\cdot^{(i)}]\right)$$
$$[\mathrm{St}]V+2k_\mathrm{fG}[\cdot S_n\cdot^{(i)}][B^*]V$$
$$-\left(k_\mathrm{fM}[\mathrm{St}]+k_\mathrm{fG}[B^*]+k_\mathrm{tc}([R\cdot]+2[\cdot R\cdot])+k''_\mathrm{tc}[P_0\cdot]\right)[S_n\cdot^{(i)}]V$$
$$+2k_\mathrm{tc}\sum_{j=0}^{i}\sum_{m=1}^{n-1}[\cdot S_{n-m}\cdot^{(i-j)}][S_m\cdot^{(j)}]V \tag{A.13}$$
$$+f_2k_{d2}\sum_{j=i+1}^{\infty}\sum_{m=n+1}^{\infty}\left(p_{mj}(n,i)j[S_m^{(j)}]+p'_\mathrm{mj}(n,i)j[P_m^{(j)}]\right)V$$

In *Eq*. (A.13), $p_{mj}(n,i)$ is the probability that a scission of a chain of dead polymer of length m and i peroxide groups yields a growing monoradical of chain length n with i peroxide groups, $p'_\mathrm{mj}(n,i)$ is the probability that a scission of a temporarily dead PS chain in the GC of length m and i peroxide groups yields a growing monoradical of chain length n with i peroxide groups.

Adding this probability over all is and ns, the following can be proved:

$$\sum_{i=1}^{\infty}\sum_{n=1}^{\infty}\sum_{j=i+1}^{\infty}\sum_{m=n+1}^{\infty}\left(p_{mj}(n,i)j[S_m^{(j)}]+p'_\mathrm{mj}(n,i)j[P_m{}^{(j)}]\right)$$
$$=\sum_{i=1}^{\infty}\sum_{n=1}^{\infty}\left(2i[S_n^{(i)}]+i[P_n^{(i)}]\right)=2[\mathrm{Pe_{PS}}]+[\mathrm{Pe_C}] \tag{A.14}$$

where $[\mathrm{Pe_{PS}}]$ is the concentration of peroxide groups in the free PS chains and $[\mathrm{Pe_C}]$ is the concentration of peroxides groups in the GC. Note that the scission of any free polystyrene chain with peroxide groups produces 2 PS monoradicals, whereas the scission of a chain within the copolymer generates only one PS monoradical and one copolymer monoradical.

For PB radicals and copolymer radicals,

$$\frac{d}{dt}\left([P_0\cdot^{(i)}]V\right)=\left(k_{i2}\sum_{j=0}^{\phi-1}\left(2[\cdot I\cdot^{(j)}]+[I\cdot^{(j)}]\right)+k_\mathrm{fG}([R\cdot]+2[\cdot R\cdot])\right)[B^*(i)]V$$
$$-\left(k_{p1}[\mathrm{St}]+k'_\mathrm{fM}[\mathrm{St}]+k'_\mathrm{tc}[P_0\cdot]+k_\mathrm{tc}([R\cdot]+2[\cdot R\cdot])\right)[P_0\cdot^{(i)}]V \tag{A.15}$$

$$\frac{d}{dt}\left([P_1\cdot^{(i)}]V\right)=k_{i1}[\mathrm{St}][P_0\cdot^{(i)}]V+2k_\mathrm{tc}\sum_{j=0}^{i}[P_0\cdot^{(i-j)}][\cdot S_1{}^{(j)}\cdot]V$$
$$-\left(k_\mathrm{p}[\mathrm{St}]+k_\mathrm{fM}[\mathrm{St}]+k_\mathrm{fG}[B^*]+k''_\mathrm{tc}[P_0\cdot]+k_\mathrm{tc}([R\cdot]+2[\cdot R\cdot])\right)[P_1\cdot^{(i)}]V \tag{A.16}$$

$$\frac{d}{dt}\left([P_n\cdot^{(i)}]V\right)=k_\mathrm{p}[\mathrm{St}][P_{n-1}\cdot^{(i)}]V$$
$$+f_2k_{d2}\sum_{j=i+1}^{\infty}\sum_{m=n+1}^{\infty}p'_\mathrm{mj}(n,i)j[P_m^{(j)}]V+2k_\mathrm{tc}\sum_{j=0}^{i}\sum_{m=1}^{n-1}[P_{n-m}\cdot^{(i-j)}][\cdot S_m\cdot^{(j)}]V$$
$$-\left(k_\mathrm{p}[\mathrm{St}]+k_\mathrm{fM}[\mathrm{St}]+k_\mathrm{fG}[B^*]+k''_\mathrm{tc}[P_0\cdot]+k_\mathrm{tc}([R\cdot]+2[\cdot R\cdot])\right)[P_n\cdot^{(i)}]V \tag{A.17}$$

where $\left[B^{*(i)}\right]$ is the molar concentration of total B units in PB or copolymer molecules with i = 0,1,2... undecomposed peroxide groups and

$$[B^*]=\sum_{i=0}^{\infty}[B^{*(i)}] \tag{A.18}$$

Note that i = 0 for PB.

Summing *Eq*. (A.15) all over is,

$$\frac{d}{dt}([P_0\cdot]V)=\left(k_{i2}\sum_{j=0}^{\phi-1}\left(2[\cdot I\cdot^{(j)}]+[I\cdot^{(j)}]\right)+k_\mathrm{fG}([R\cdot]+2[\cdot R\cdot])\right)[B^*]V$$
$$-\left(k_{i1}[\mathrm{St}]+k'_\mathrm{fM}[\mathrm{St}]+k'_\mathrm{tc}[P_0\cdot]+k_\mathrm{tc}([R\cdot]+2[\cdot R\cdot])\right)[P_0\cdot]V \tag{A.19}$$

From *Eqs*. (A.16) and (A.17), summing all over ns and is, the total concentration of PB and copolymer radicals may be obtained:

$$\frac{d}{dt}([P\cdot]V)=k_{i1}[\mathrm{St}][P_0\cdot]V+k_\mathrm{fG}([S\cdot]+2[\cdot R\cdot])[B^*]V+k_{d2}[\mathrm{Pe_C}]V$$
$$-\left(k_\mathrm{fM}[\mathrm{St}]+k''_\mathrm{tc}[P_0\cdot]+k_\mathrm{tc}([S\cdot]+[P\cdot])\right)[P\cdot]V \tag{A.20}$$

From *Eqs*. (A.10) and (A.12), the total concentration of diradicals (which are only PS homoradicals) may be obtained:

$$\frac{d}{dt}([\cdot R\cdot]V)=k_{i2}\sum_{j=0}^{\phi-1}2[\cdot I\cdot^{(j)}][\mathrm{St}]V+2k_\mathrm{tc}[\cdot R\cdot]^2V$$
$$-2\left(k_\mathrm{fM}[\mathrm{St}]+k_\mathrm{fG}[B^*]+k_\mathrm{tc}([R\cdot]+2[\cdot R\cdot])+k''_\mathrm{tc}[P_0\cdot]\right)[\cdot R\cdot]V \tag{A.21}$$

From *Eqs*. (A.11) and (A.13) and considering *Eq*. (A.14) the total concentration of PS monoradicals may be obtained:

$$\frac{d}{dt}([S\cdot]V)= \left. k_{i2}\sum_{j=0}^{\phi-1}[I\cdot^{(j)}]+k_{\mathrm{fM}}([P\cdot]+4[\cdot R\cdot])\right)[\mathrm{St}]V+2k_i[\mathrm{St}]^3V$$
$$+2k_{\mathrm{fG}}[B^*][\cdot R\cdot]V$$
$$-\left(k_{\mathrm{tc}}([S\cdot]+[P\cdot]+2[\cdot R\cdot])+k_{\mathrm{fG}}[B^*]+k''_{\mathrm{tc}}[P_0\cdot]\right)[S\cdot]V$$
$$+f_2k_{d2}(2[\mathrm{Pe_{PS}}]+[\mathrm{Pe_C}])V \tag{A.22}$$

The total radicals are calculated as $[R\cdot]+2[\cdot R\cdot]=[S\cdot]+[P\cdot]+2[\cdot R\cdot]$. Using *Eqs*. (A.20) through (A.22),

$$\frac{d}{dt}(([R\cdot]+2[\cdot R\cdot])V)=k_{i1}\sum_{j=0}^{\phi-1}\left(4[\cdot I\cdot^{(j)}]+[I\cdot^{(j)}]\right)[\mathrm{St}]V$$
$$+2k_i[\mathrm{St}]^3V+k_{i1}[\mathrm{St}][P_0\cdot]V \tag{A.23}$$
$$+2f_2k_{d2}([\mathrm{Pe_{PS}}]+[\mathrm{Pe_C}])V-k_{\mathrm{tc}}([R\cdot]+2[\cdot R\cdot])^2V$$
$$-k''_{\mathrm{tc}}([R\cdot]+2[\cdot R\cdot])[P_0\cdot]V$$

Peroxide Groups. Neglecting the concentration of peroxide groups in the radicals, the total concentration of peroxide groups is

$$[\mathrm{Pe}]=\sum_{j=1}^{\phi}j\left([I^{(j)}]+[\bar{I}^{(j)}]\right)+[\mathrm{Pe_{PS}}]+[\mathrm{Pe_C}] \tag{A.24}$$

with

$$[\mathrm{Pe_{PS}}]=\sum_{i=0}^{\infty}\sum_{n=1}^{\infty}i\left[S_n{}^{(i)}\right] \tag{A.25a}$$

$$[\mathrm{Pe_C}]=\sum_{i=0}^{\infty}i\left[P^{(i)}\right] \tag{A.25b}$$

Peroxide groups are consumed only by decomposition reactions. Therefore,

$$\frac{d}{dt}([\mathrm{Pe}]V)=-\sum_{i=1}^{\phi}jk_{d1}\left([I^{(i)}]+[\bar{I}^{(i)}]\right)V-k_{d2}([\mathrm{Pe_{PS}}]+[\mathrm{Pe_C}])V \tag{A.26}$$

Using this result and *Eq*. (A.24), the molar concentration of peroxide groups accumulated in the free PS and the GC can be calculated from the following difference

$$\frac{d}{dt}(\{[\mathrm{Pe_{PS}}]+[\mathrm{Pe_C}]\}V)=\frac{d}{dt}([\mathrm{Pe}]V)-\sum_{j=1}^{\phi}j\frac{d}{dt}\left(\left([I^{(j)}]+[\bar{I}^{(j)}]\right)V\right) \tag{A.27}$$

Conversion and Volume. Monomer conversion can be calculated from

$$x=\frac{[\mathrm{St}]_0V_0-[\mathrm{St}]V}{[\mathrm{St}]_0V_0} \tag{A.28}$$

where the subscript "0" indicates initial conditions.

The evolution of the reaction volume V is obtained as in Estenoz et al. from

$$V=V_0^{\mathrm{St}}(1-\varepsilon x)+V_0^{\mathrm{PB}} \tag{A.29}$$

with

$$\varepsilon=\frac{V_0^{\mathrm{St}}-V_{\mathrm{f}}^{\mathrm{S}}}{V_0^{\mathrm{St}}} \tag{A.30}$$

where ε is the St volume contraction factor, V_0^{St} and V_0^{PB} are the initial St and PB volumes respectively and $V_{\mathrm{f}}^{\mathrm{S}}$ is the final volume of free and grafted St at full conversion.

Equations (A.1)–(A.6), (A.8), (A.9), (A.19), (A.23)–(A.29) are solved simultaneously to find the evolution of $[I^{(i)}]$, $[\bar{I}^{(i)}]$, [St], $[B^*]$, $[\cdot I\cdot^{(i)}]$, $[I\cdot^{(i)}]$, $[P_0\cdot]$, $([R\cdot]+2[\cdot R\cdot])$, $([\mathrm{Pe_{PS}}]+[\mathrm{Pe_C}])$, x and V.

APPENDIX B: DISTRIBUTIONS MODULE

Free PS

Radical Species ($i=\mathbf{0},\mathbf{1},\ldots;n=\mathbf{2},\mathbf{3},\ldots$)**.** Consider equations (A.17) and (A.10). Assuming pseudosteady-state, all time derivatives may be set to zero and the following recurrence formulas can be obtained:

$$[\cdot S_n\cdot^{(i)}]=\frac{k_{\mathrm{p}}[\mathrm{St}][\cdot S_{n-1}\cdot^{(i)}]+k_{\mathrm{tc}}\sum_{j=0}^{i}\sum_{m=1}^{n-1}[\cdot S_{n-m}\cdot^{(i-j)}][\cdot S_m\cdot^{(j)}]}{k_{\mathrm{p}}[\mathrm{St}]+k_{\mathrm{fM}}[\mathrm{St}]+k_{\mathrm{fG}}[B^*]+k_{\mathrm{tc}}([R\cdot]+2[\cdot R\cdot])+k''_{\mathrm{tc}}[P_0\cdot]} \tag{B.1}$$

$$[S_n\cdot^{(i)}]=\frac{\left(k_{\mathrm{p}}[S_{n-1}\cdot^{(i)}]+2k_{\mathrm{fM}}[\cdot S_n\cdot^{(i)}]\right)[\mathrm{St}]+2k_{\mathrm{fG}}[\cdot S_n\cdot^{(i)}][B^*]}{k_{\mathrm{p}}[\mathrm{St}]+k_{\mathrm{fM}}[\mathrm{St}]+k_{\mathrm{fG}}[B^*]+k_{\mathrm{tc}}([R\cdot]+2[\cdot R\cdot])+k''_{\mathrm{tc}}[P_0\cdot]}$$
$$+\frac{2k_{\mathrm{tc}}\sum_{j=0}^{i}\sum_{m=1}^{n-1}[\cdot S_{n-m}\cdot^{(i-j)}][S_m\cdot^{(j)}]+k_{d2}\sum_{j=i+1}^{\infty}\sum_{m=n+1}^{\infty}\left(p_{mj}(n,i)j[S_m^{(j)}]+p'_{\mathrm{mj}}(n,i)j[P_m^{(j)}]\right)}{k_{\mathrm{p}}[\mathrm{St}]+k_{\mathrm{fM}}[\mathrm{St}]+k_{\mathrm{fG}}[B^*]+k_{\mathrm{tc}}([R\cdot]+2[\cdot R\cdot])+k''_{\mathrm{tc}}[P_0\cdot]} \tag{B.2}$$

Polystyrene Species ($i=\mathbf{0},\mathbf{1},\ldots;n=\mathbf{2},\mathbf{3},\ldots$)**.** The mass balances for the PS species provide

$$\frac{d}{dt}\left([S_n{}^{(i)}]V\right)=k_{\mathrm{fM}}[\mathrm{St}][S_n\cdot^{(i)}]V$$
$$+\frac{k_{\mathrm{tc}}}{2}\sum_{j=0}^{i}\sum_{m=1}^{n-1}[S_{n-m}\cdot^{(i-j)}][S_m\cdot^{(j)}]V-i\,k_{d2}[S_n{}^{(i)}]V \tag{B.3}$$
$$+(1-f_2)k_{d2}\sum_{j=i+1}^{\infty}\sum_{m=n+1}^{\infty}\left(p_{mj}(n,i)j[S_m^{(j)}]+p'_{mj}(n,i)j[P_m^{(j)}]\right)V$$

In order to account for the generation of monoradicals from random scission of the Free PS or graft copolymer chains by sequential decomposition of peroxide groups within the chains, consider a polymer chain with length n and i peroxide groups, all of which have the same thermal stability.

Let m be a uniformly distributed random variable whose value ranges 1 from 1 to $n-1$. The polymer chain may

form 2 monoradicals, one with length m, and the other one with length $n - m$. These chains will have $i - j$ and $j - 1$ undecomposed peroxide groups respectively. If the peroxide groups are uniformly distributed in the formed monoradicals, the following relation must hold:

$$\frac{j-1}{n-m}=\frac{i-j}{m}$$

Therefore,

$$j=\left[\frac{i(n-m)+m}{n}\right]$$

where the brackets indicate the integer part of the expression.

The scission has then generated two monoradicals, one with length m and i-j peroxide groups, the other one with length $n - m$ and $j - 1$ peroxide groups.

This scission must be performed for all polymer chains whose peroxide group number is greater than 0.

The Number Chain Length Distribution (NCLD) for the free PS species is

$$N_{\mathrm{PS}}^{(i)}(n)=[S_n^{(i)}]V \tag{B.4}$$

Found by integrating *Eq. B.3* with *Eqs. B.1* and *B.2*.

The concentration of the total PS species characterized by the number of undecomposed peroxide groups can be calculated with

$$[P^{(i)}]=\sum_{n=1}^{\infty}[S_n^{(i)}] \tag{B.5}$$

To obtain the corresponding weight chain length distribution (WCLD), multiply the NCLD by sM_{St} and replace n by s to obtain

$$G_{\mathrm{PS}}^{(i)}(s)=sM_{\mathrm{St}}[S_s^{(i)}]V \tag{B.6}$$

The mass of free PS can then be calculated as:

$$G_{\mathrm{PS}}=\sum_{i=0}^{\infty}\sum_{s=1}^{\infty}G_{\mathrm{PS}}^{(i)}(s) \tag{B.9}$$

The average molecular weights can then be calculated from

$$\bar{M}_{\mathrm{n,PS}}=\frac{G_{\mathrm{PS}}}{N_{\mathrm{PS}}}=\frac{\sum_{i=0}^{\infty}\sum_{s=1}^{\infty}G_{\mathrm{PS}}^{(i)}(s)}{\sum_{i=0}^{\infty}\sum_{n=1}^{\infty}[S_n{}^{(i)}]V} \tag{B.10a}$$

$$\bar{M}_{w,\mathrm{PS}}=\frac{\sum_{i=0}^{\infty}\sum_{s=1}^{\infty}sG_{\mathrm{PS}}^{(i)}(s)}{G_{\mathrm{PS}}}=\frac{\sum_{i=0}^{\infty}\sum_{s=1}^{\infty}sG_{\mathrm{PS}}^{(i)}(s)}{\sum_{i=0}^{\infty}\sum_{s=1}^{\infty}G_{\mathrm{PS}}^{(i)}(s)} \tag{B.10b}$$

Residual PB. Let $N_{\mathrm{PB}}(b)$ denote the moles of PB with b units of B $(b \geq 1)$. Consider only the reactions involving the unreacted PB and the reactions at each chain length b, $bN_{\mathrm{PB}}(b)$ is therefore the molar concentrations of B^* at each chain length. Assuming that the number of attacked B^* is proportional to the B^* contents of each chain length class, the fraction of $P_0\cdot$ radicals that are primary PB radicals of chain length b is therefore $bN_{\mathrm{PB}}(b)/[B^*]$.

Then, from the kinetic mechanism,

$$\frac{d}{dt}N_{\mathrm{PB}}(b)=-\left(k_{i2}\sum_{j=0}^{\phi-1}\left(2[\cdot I\cdot^{(j)}]+[I\cdot^{(j)}]\right)+k_{\mathrm{fG}}([R\cdot]+2[\cdot R\cdot])\right)$$
$$bN_{\mathrm{PB}}(b)+k'_{\mathrm{fM}}[\mathrm{St}][P_0\cdot]\frac{bN_{\mathrm{PB}}(b)}{[B^*]} \tag{B.11}$$

where $N_{\mathrm{PB}}(b)$ at $t = 0$ is *a priori* known from experimental data.

The corresponding WCLD for the residual PB can be obtained from

$$G_{\mathrm{PB}}(b)=bM_{\mathrm{B}}N_{\mathrm{PB}}(b) \tag{B.12}$$

The total moles and mass of the residual PB are therefore

$$N_{\mathrm{PB}}=\sum_{b=1}^{\infty}N_{\mathrm{PB}}(b) \tag{B.13}$$

$$G_{\mathrm{PB}}=\sum_{b=1}^{\infty}G_{\mathrm{PB}}(b) \tag{B.14}$$

Grafting Efficiency and Average Number of St Branches. The grafted St mass G_{GS} can be calculated from

$$G_{\mathrm{GS}}=M_{\mathrm{St}}[\mathrm{St}]_0V_0x-G_{\mathrm{PS}} \tag{B.15}$$

The St grafting efficiency is calculated from

$$E_{\mathrm{GS}}=\frac{G_{\mathrm{GS}}}{G_{\mathrm{PS}}+G_{\mathrm{GS}}} \tag{B.16}$$

The average number of St branches per reacted PB molecule is

$$J=\frac{G_{\mathrm{GS}}/\bar{M}_{n,\mathrm{PS}}}{N_{\mathrm{PB}_0}-N_{\mathrm{PB}}} \tag{B.17}$$

Phase Volumes. The volume of the individual phases, considered completely immiscible, is obtained from

$$V_{\mathrm{I}}=\frac{G_{\mathrm{PB}}+G_{\mathrm{GS}}}{\rho_{\mathrm{PB}}} \tag{B.18a}$$

$$V_{\mathrm{II}}=\frac{M_{\mathrm{St}}[\mathrm{St}]\mathrm{V}_{\mathrm{II}}\rho_{\mathrm{St}}+\mathrm{G}_{\mathrm{PS}}}{\rho_{\mathrm{PS}}} \tag{B.18b}$$

where ρ_k is the density of chemical species k.

Graft Copolymer. The complete copolymer distribution, characterized by grafted St and B units in the copolymer and number of undecomposed peroxide groups, is derived from the detailed kinetic mechanism in Table D1 for copolymer

radicals and copolymer species. The following nomenclature was used:

$P^{(i)}(s,b)$	Copolymer with s styrene units, b butadiene units and i undecomposed peroxide groups in the grafted chains
$P_0{\cdot}^{(i)}(s,b)$	Primary Radical produced by attack to a butadiene repetitive unit (B) present $P^{(i)}(s,b)$
$P_n{\cdot}^{(i)}(s,b)$	Copolymer radical with i undecomposed peroxide groups s styrene units, b butadiene units and n units of St in the active branch

Copolymer Radicals. For deriving the equations, it was considered that $[B^*(i)(s,b)] \approx b[P^{(i)}(s,b)]$. From the detailed kinetic mechanism of Table B1 and using the pseudosteady-state hypothesis,

$$\left(k_{i2}\sum_{j=0}^{\phi-1}\left(2[\cdot I^{(j)}\cdot]+[I^{(j)}\cdot]\right)+k_{\mathrm{fG}}([R\cdot]+2[\cdot R\cdot])\right)b[P^{(i)}(s,b)]$$
$$-\left(k_{i1}[\mathrm{St}]+k'_{\mathrm{fM}}[\mathrm{St}]+k'_{\mathrm{tc}}[P_0\cdot]+k''_{\mathrm{tc}}([R\cdot]+2[\cdot R\cdot])\right)[P_0{\cdot}^{(i)}(s,b)]=0 \tag{B.19}$$

$$k_{i1}[\mathrm{St}][P_0{\cdot}^{(i)}(s,b)]+2k''_{\mathrm{tc}}\sum_{j=0}^{i}[P_0{\cdot}^{(i-j)}(s,b)][\cdot S_1{}^{(j)}\cdot]$$
$$-\left(k_{\mathrm{p}}[\mathrm{St}]+k_{\mathrm{fM}}[\mathrm{St}]+k_{\mathrm{fG}}[B^*]+k'_{\mathrm{tc}}[P_0\cdot]+k''_{\mathrm{tc}}([R\cdot]+2[\cdot R\cdot])\right) \tag{B.20}$$
$$[P_1{\cdot}^{(i)}(s,b)]V=0$$

$$k_{\mathrm{p}}[\mathrm{St}][P_{n-1}{\cdot}^{(i)}(s,b)]+f_2k_{d2}\sum_{j=i+1}^{\infty}\sum_{m=n+1}^{\infty}\sum_{t=s+1}^{\infty}\sum_{c=b}^{\infty}p''_{mjtc}(n,i,s,b)j[P_m^{(j)}(t,c)]+$$
$$2k''_{\mathrm{tc}}\sum_{j=0}^{i}\sum_{m=1}^{n-1}[P_{n-m}{\cdot}^{(i-j)}(s,b)][\cdot S_m{\cdot}^{(j)}]V+2k''_{\mathrm{tc}}\sum_{j=0}^{i}[P_0{\cdot}^{(i-j)}(s,b)][\cdot S_n{\cdot}^{(j)}]$$
$$-\left(k_{\mathrm{p}}[St]+k_{\mathrm{fM}}[St]+k_{\mathrm{fG}}[B^*]+k'_{\mathrm{tc}}[P_0\cdot]+k''_{\mathrm{tc}}([R\cdot]+2[\cdot R\cdot])\right)[P_n{\cdot}^{(i)}(s,b)]=0 \tag{B.21}$$

In *Eq.* (B.21) $p''_{mjtc}(n,i,s,b)$ is the probability that a scission of a temporarily dead PS chain from $P^{(j)}(t,c)$ having m repetitive units of St and j peroxide groups yields a growing PS monoradical of chain length n with i peroxide groups, with the resulting copolymer radical having s units of St and b units of B.

Copolymer Bivariate Distribution.

$$\frac{d}{dt}\left(\left[P^{(i)}(s,b)\right]V\right)=-k_{i2}\sum_{j=0}^{\phi-1}\left(2\left[\cdot I^{(j)}\cdot\right]+\left[I^{(j)}\cdot\right]\right)b\left[P^{(i)}(s,b)\right]V$$
$$-k_{\mathrm{fG}}([R\cdot]+2[\cdot R\cdot]+[P_0\cdot])b\left[P^{(i)}(s,b)\right]V-ik_{d2}f_2\left[P^{(i)}(s,b)\right]V$$
$$+(1-f_2)k_{d2}\sum_{j=i+1}^{\infty}\sum_{t=s+1}^{\infty}p'_{jt}(i,s)j\left[P^{(j)}(t,b)\right]V$$
$$+k_{\mathrm{fG}}[B^*]\sum_{n=1}^{s}[P_n^{(i)}\cdot(s-n,b)]V+k_{\mathrm{fG}}[B^*][P_0^{(i)}\cdot(s,b)]V$$
$$+k_{\mathrm{fM}}[St]\sum_{n=1}^{s}[P_n^{(i)}\cdot(s-n,b)]V+k_{\mathrm{fM}}[St][P_0^{(i)}\cdot(s,b)]V$$
$$+\frac{1}{2}k'_{\mathrm{tc}}\sum_{j=0}^{i}\sum_{t=0}^{s}\sum_{c=1}^{b-1}\left[P_0^{(i-j)}\cdot(s-t,b-c)\right]\left[P_0^{(j)}\cdot(t,c)\right]V$$
$$+k'_{\mathrm{tc}}\sum_{m=1}^{s-t}\sum_{t=0}^{s-1}\sum_{j=0}^{i}\sum_{c=1}^{b-1}\left[P_0^{(i-j)}\cdot(s-t-m,b-c)\right]\left[P_m^{(j)}\cdot(t,c)\right]V$$
$$+\frac{1}{2}k'_{\mathrm{tc}}\sum_{n=1}^{s-t-m}\sum_{m=1}^{s-t}\sum_{t=0}^{s-1}\sum_{j=0}^{i}\sum_{c=1}^{b-1}\left[P_n^{(i-j)}\cdot(s-t-m-n,b-c)\right]\left[P_m^{(j)}\cdot(t,c)\right]V$$
$$+k''_{\mathrm{tc}}\sum_{j=0}^{i}\sum_{n=1}^{s}\left[P_0^{(i-j)}\cdot(s-n,b)\right]\left[S_n^{(j)}\cdot\right]V$$
$$+k''_{\mathrm{tc}}\sum_{n=1}^{s-m}\sum_{m=1}^{s-1}\sum_{j=0}^{i}\left[P_m^{(i-j)}\cdot(s-n-m,b)\right]\left[S_n^{(j)}\cdot\right]V \tag{B.22}$$

The total copolymer NCLD can be obtained from

$$N(s,b)=\sum_{i=0}^{\infty}P^{(i)}(s,b)V \tag{B.23}$$

and the corresponding WCLD from

$$G(s,b)=(sM_{\mathrm{St}}+bM_{\mathrm{B}})N(s,b) \tag{B.24}$$

TABLE B1. Detailed kinetic mechanism for copolymer bivariate distribution.

Initiation ($\phi=1,2,3; i<\phi; j=0,1,\ldots; s,b=1,2,\ldots$)

$\cdot I^{(i)}+P^{(j)}(s,b)\xrightarrow{2k_{i2}}P_0{\cdot}^{(j)}(s,b)+I^{(i)}$

$I^{(i)}+P^{(j)}(s,b)\xrightarrow{k_{i2}}P_0{\cdot}^{(j)}(s,b)+\bar{I}^{(i)}$

Propagation ($n,s,b=1,2,3\ldots; i=0,1,2\ldots$)

$P_0{\cdot}^{(i)}(s,b)+\mathrm{St}\xrightarrow{k_{\mathrm{p}}}P_1{\cdot}^{(i)}(s,b)$

$P_n{\cdot}^{(i)}(s,b)+\mathrm{St}\xrightarrow{k_{\mathrm{p}}}P_{n+1}{\cdot}^{(i)}(s,b)$

Transfer to monomer ($n,s,b=1,2,3\ldots; i=0,1,2\ldots$)

$P_0{\cdot}^{(i)}(s,b)+\mathrm{St}\xrightarrow{k'_{\mathrm{fM}}}P^{(i)}(s,b)+S_1{\cdot}^{(0)}$

$P_n{\cdot}^{(i)}(s-n,b)+\mathrm{St}\xrightarrow{k_{\mathrm{fM}}}P^{(i)}(s,b)+S_1{\cdot}^{(0)}$

Transfer to rubber ($n,s,b,c,t=1,2,3\ldots; i,j=0,1,2\ldots$)

$S_n{\cdot}^{(i)}+P^{(j)}(s,b)\xrightarrow{k_{\mathrm{fG}}}S_n{}^{(i)}+P_0{\cdot}^{(j)}(s,b)$

$\cdot S_n{\cdot}^{(i)}+P^{(j)}(s,b)\xrightarrow{2k_{\mathrm{fG}}}S_n{\cdot}^{(i)}+P_0{\cdot}^{(j)}(s,b)$

$P_0{\cdot}^{(i)}(s,b)+P^{(j)}(t,c)\xrightarrow{k_{\mathrm{fG}}}P^{(i)}(s,b)+P_0{\cdot}^{(j)}(t,c)$

$P_n{\cdot}^{(i)}(s-n,b)+P^{(j)}(t,c)\xrightarrow{k_{\mathrm{fG}}}P^{(i)}(s,b)+P_0{\cdot}^{(j)}(t,c)$

Re-initiation ($s,b=1,2,3,\ldots; n=1,2,\ldots,s-1; m=1,2,\ldots,n-1;$ $i=1,2\ldots; j=0,1,\ldots,i-1$)

$P^{(i)}(s,b)\xrightarrow{ik_{\mathrm{dp}}}P_{n-m}{\cdot}^{(i-j)}(s-n-m,b)+S_m{}^{(j-1)}\cdot$

Termination by combination ($n,m,s,b,c,t=1,2,3\ldots; i,j=0,1,2\ldots$)

$P_0{\cdot}^{(i-j)}(s-t,b-c)+P_0{\cdot}^{(j)}(t,c)\xrightarrow{k'_{\mathrm{tc}}}P^{(i)}(s,b)$

497:29

$P_n{\cdot}^{(i-j)}(s-n-m-t,b-c)+P_m{\cdot}^{(j)}(t,c)\xrightarrow{k'_{\mathrm{tc}}}P^{(i)}(s,b)$

$P_0{\cdot}^{(i-j)}(s,b)+\cdot S_m{\cdot}^{(j)}\xrightarrow{2k''_{\mathrm{tc}}}P_m{\cdot}^{(i)}(s,b)$

$P_n{\cdot}^{(i-j)}(s,b)+\cdot S_m{\cdot}^{(j)}\xrightarrow{2k''_{\mathrm{tc}}}P_{n+m}{\cdot}^{(i)}(s,b)$

$P_0{\cdot}^{(i-j)}(s-m,b)+S_m{\cdot}^{(j)}\xrightarrow{k''_{\mathrm{tc}}}P^{(i)}(s,b)$

$P_n{\cdot}^{(i-j)}(s-n-m,b)+S_m{\cdot}^{(j)}\ +\ \xrightarrow{k''_{\mathrm{tc}}}\ P^{(i)}(s,b)$

Copolymer Average Composition and Molecular Weights. The average chemical composition of the graft copolymer is estimated with the mass fraction of St

$$\bar{\omega}_{St}=\frac{\sum_{i=0}^{\infty}\sum_{s=1}^{\infty}\sum_{b=1}^{\infty}[P^{(i)}(s,b)]sM_{St}}{\sum_{i=0}^{\infty}\sum_{s=1}^{\infty}\sum_{b=1}^{\infty}[P^{(i)}(s,b)](sM_{St}+bM_{Bd})} \tag{B.25}$$

The copolymer average molecular weights are calculated with

$$\bar{M}_{n,C}=\frac{\sum_{i=0}^{\infty}\sum_{b=1}^{\infty}\sum_{s=1}^{\infty}[P^{(i)}(s,b)](sM_{St}+bM_{B})}{\sum_{i=0}^{\infty}\sum_{b=1}^{\infty}\sum_{s=1}^{\infty}[P^{(i)}(s,b)]} \tag{B.26a}$$

$$\bar{M}_{w,C}=\frac{\sum_{i=0}^{\infty}\sum_{b=1}^{\infty}\sum_{s=1}^{\infty}[P^{(i)}(s,b)](sM_{St}+bM_{B})^{2}}{\sum_{i=0}^{\infty}\sum_{b=1}^{\infty}\sum_{s=1}^{\infty}[P^{(i)}(s,b)](sM_{St}+bM_{B})} \tag{B.27a}$$

APPENDIX C: MELT FLOW INDEX MODULE

The melt flow index (MFI) is the mass flow rate, in units of g/10 min, of a HIPS melt that flows through a plastometer capillary when forced by a piston loaded with constant weight. The polymer accumulates in a barrel, prior to entering the capillary. Between the barrel and the capillary there is an abrupt contraction or "entrance" zone.

First, the apparent shear viscosity $\eta(\dot{\gamma})$ is related to the apparent shear rate $\dot{\gamma}$ by means of a three-parameter Carreau expression [36, 37].

$$\eta(\dot{\gamma})=\frac{\eta_0}{\left[1+(\tau_r\dot{\gamma})^2\right]^{n'/2}} \tag{C.1}$$

where η_0 is the zero-shear viscosity, τ_r the relaxation time and n' is a rheological parameter [38]. The relaxation time of the polymer is calculated as:

$$\tau_r=\frac{6\eta_{0,P}\bar{M}_{w,PS}}{\pi^2\rho RT} \tag{C.2}$$

For $\eta_{0,P}$, the polymer shear viscosity, the following expression is used

$$\eta_{0,P}=\eta_{0,PS}e^{\frac{A\phi_D}{1-B\phi_D}} \tag{C.3}$$

where $\eta_{0,PS}$ is the zero-shear viscosity of the free PS, A and B are constants taken from the literature [39] and ϕ_D is the volume fraction of the dispersed phase, which is estimated as $\phi_D \approx \phi_R$ where ϕ_R is the total rubber in the final product, calculated as

$$\phi_R=\frac{\sum_{i=PB,GC}G_i/\rho_i}{\sum_{i=PS,PB,GC}G_i/\rho_i} \tag{C.4}$$

This approximation estimates ϕ_D by defect, since ϕ_R does not include the occluded PS contained in the rubber particles [25]. Finally, $\eta_{0,PS}$ is estimated from

$$\ln\eta_{0,PS}=-20.95+3.4\ln\left(\frac{\bar{M}_{w,PS}}{33000}\right)+\frac{11000}{T} \tag{C.5}$$

The MFI is estimated using the model proposed by Seavey et al. [40] The model assumes: (a) steady-state flow; (b) zero velocity at the capillary wall; and (c) the elongational viscosity can be estimated using Trouton's ratio. While assumption (b) is valid for homogeneous systems [35], it is extended here to an heterogeneous one. The following nomenclature was used:

R_b	Barrel radius
L_b	Barrel length
R_c	Capillary radius
L_c	Capillary length
R_p	Piston radius
ΔP_b	Pressure drop in the barrel
ΔP_c	Pressure drop in the capillary
ΔP_e	Pressure drop in the entrance zone
$\dot{\gamma}_{R_b}$	Shear rate at the barrel wall
$\dot{\gamma}_{R_c}$	Shear rate at the capillary wall
$\dot{\epsilon}_a$	Apparent elongational rate in the capillary
η_{R_b}	Apparent viscosity at the barrel wall
η_{R_c}	Apparent viscosity at the capillary wall
η_{e_c}	Apparent elongational viscosity in the capillary
m	Piston weight
g	Acceleration of gravity
ΔP_b	Shear rate at the barrel wall

The MFI is calculated as

$$MFI=\rho\dot{Q} \tag{C.6}$$

where $\dot{Q}$ is the volumetric flow rate through the plastometer, and ρ is the density of the final HIPS, calculated as

$$\rho=\sum_{i=PS,PB,GC}\omega_i\rho_i \tag{C.7}$$

where the ω_i are the mass fractions of the different polymer species.

The volumetric flow $\dot{Q}$ is calculated from the relation between η and $\dot{\gamma}$ given by *Eq.* (C.1) and the following mass and momentum balances in the plastometer [35, 41]

$$\dot{Q}=\frac{\pi R_b^3\dot{\gamma}_{R_b}}{3}-\frac{\pi}{3}\left(\frac{2L_b}{\Delta P_b}\right)^3\int_0^{\dot{\gamma}_{R_b}}[\eta(\dot{\gamma})\dot{\gamma}]^3d\dot{\gamma} \tag{C.8}$$

$$\dot{Q}=\frac{\pi R_c^3\dot{\gamma}_{R_c}}{3}-\frac{\pi}{3}\left(\frac{2L_c}{\Delta P_c}\right)^3\int_0^{\dot{\gamma}_{R_c}}[\eta(\dot{\gamma})\dot{\gamma}]^3d\dot{\gamma} \tag{C.9}$$

$$\dot{\gamma}_{R_b}\eta_{R_b}=\frac{\Delta P_b R_b}{2L_b} \tag{C.10}$$

$$\dot{\gamma}_{R_c}\eta_{R_c}=\frac{\Delta P_c R_c}{2L_c} \tag{C.11}$$

The total pressure drop is given by

$$\Delta P_b + \Delta P_e + \Delta P_c = \frac{mg}{\pi R_p^2} \tag{C.12}$$

where ΔP_e is estimated as in the work of Rohlfing and Janzen [41]:

$$\Delta P_e = \frac{4\sqrt{2}\dot{\gamma}_a}{3(n'+1)} \left(\frac{4n'}{3n'+1}\right)^{(1+n'/2)} \sqrt{\eta_{a,c}\eta_{e,c}} \tag{C.13}$$

The expressions for $\dot{\gamma}_a$ and $\dot{\epsilon}_a$ are

$$\dot{\gamma}_a = \left(\frac{4}{3+1/n'}\right)\dot{\gamma}_{R_c} \tag{C.14}$$

$$\dot{\epsilon}_a = \frac{4\eta_{a,c}\dot{\gamma}_a}{3(n'+1)\Delta P_e} \left(\frac{4n'}{3n'+1}\right)^{n'+1} \tag{C.15}$$

where the Trouton ratio is used to relate the elongational viscosity to the shear viscosity

$$\eta_e(\dot{\epsilon}) = 3\eta(\dot{\gamma}) \tag{C.16}$$

with $\dot{\gamma} = \epsilon_a$ [35].

The values for the numerical parameters related to plastometer geometry are: $R_b = 4.78$ mm, $R_c = 1.05$ mm, $R_p = 4.74$ mm, $L_b = 46$ mm, $L_c = 8$ mm, $m = 5$ kg and $g = 9.81$ m/s^2 with an essay temperature of $T = 200$°C. *Equations* (C.8) to (C.15) are simultaneously solved to evaluate the MFI with *Eq*. (C.6).